



Facet-dependent $\text{Cu}_2\text{O}@\text{Zn}(\text{OH})_2$ composites with enhanced visible-light photocatalysis

Lin Cheng, Guosong Wu, Aiping Liu^{*}

Key Laboratory of Optical Field Manipulation of Zhejiang Province, School of Materials Science & Engineering, Zhejiang Sci-Tech University, Hangzhou 310018, China

ARTICLE INFO

Keywords:

$\text{Cu}_2\text{O}@\text{Zn}(\text{OH})_2$ composites
Crystal structure
Surfaces
Photocatalysis

ABSTRACT

Facet-dependent $\text{Cu}_2\text{O}@\text{Zn}(\text{OH})_2$ composites were synthesized by wrapping morphology-controllable Cu_2O crystals (cubic, cuboctahedral and octahedral) with the adsorbent $\text{Zn}(\text{OH})_2$ nanosheets. The cuboctahedral $\text{Cu}_2\text{O}@\text{Zn}(\text{OH})_2$ composite exhibits the highest photocatalytic performance than cubic and octahedral ones with the degradation rate of methyl orange up to 96.6% under visible-light irradiation due to the best crystal facet-dependent photocatalytic performance of cuboctahedral Cu_2O . Moreover, the presence of $\text{Zn}(\text{OH})_2$ nanosheets can enhance the rapid adsorption of dye molecules, and thus accelerate the photocatalytic process. The combination of $\text{Zn}(\text{OH})_2$ nanosheets with physical adsorption capacity and facet-dependent Cu_2O crystals with catalytic performance effectively enhances the photocatalytic performance of composite catalyst.

1. Introduction

Cu_2O is a p-type semiconductor with a band gap energy of 2.2 eV, which is considered to have broad application prospects in solar cells, gas sensing and catalysis [1]. At present, Cu_2O particles with different morphologies such as cubic, spherical, octahedral, and other polyhedral have been synthesized [2,3], and many studies have shown that the facet-dependent Cu_2O has different photocatalytic properties [4]. Higher energy crystal facets are beneficial to improve the catalytic performance, and the difference of surface energy between different facets can accelerate the separation of photo-excited electron-hole pairs, presenting the general order of photocatalytic activity of $\{110\}$ faces $> \{111\}$ faces $> \{100\}$ faces [5]. Thus, the photocatalytic performance of Cu_2O can usually be improved by means of its morphology and crystalline structure control. Additionally, $\text{Zn}(\text{OH})_2$ has been proved to have potential application as adsorption material due to its large specific surface area, high porosity, good reproducibility and low price [6]. Therefore, the combination of $\text{Zn}(\text{OH})_2$ materials with strong adsorption capacity and Cu_2O particles with different surface morphologies is of research significance to explore into the synergy of two ingredients on photocatalytic performance improvement of composite catalyst.

Herein, Cu_2O with desired crystal facets, namely cubic Cu_2O with $\{100\}$ facets, octahedral Cu_2O with $\{111\}$ facets and cuboctahedral Cu_2O with both $\{111\}$ and $\{100\}$ facets were fabricated respectively. Then, a layer of $\text{Zn}(\text{OH})_2$ nanosheets was coated on the surface of Cu_2O

crystal. The obtained $\text{Cu}_2\text{O}@\text{Zn}(\text{OH})_2$ composite exhibited enhanced catalytic degradation performance to methyl orange (MO) when compared with the single Cu_2O crystal. This strategy cleverly utilizes the adsorption capacity of $\text{Zn}(\text{OH})_2$ sheets to continuously provide MO molecules to contact with Cu_2O during the catalytic degradation process, thereby effectively improving the photocatalytic degradation performance of composite. In addition, the catalytic performance of $\text{Cu}_2\text{O}@\text{Zn}(\text{OH})_2$ composites with different Cu_2O morphologies were also compared, proving better catalytic activity of cuboctahedral $\text{Cu}_2\text{O}@\text{Zn}(\text{OH})_2$ when compared to the other two composites.

2. Experimental section

The synthetic procedures of morphology-controllable Cu_2O crystals [7] and $\text{Cu}_2\text{O}@\text{Zn}(\text{OH})_2$ composites, and detailed characterization methods were described in the Supportive information.

3. Results and discussion

Fig. 1a–c show the morphology-controllable Cu_2O crystals with good regularity and uniformity. The $\text{Cu}_2\text{O}@\text{Zn}(\text{OH})_2$ composites also present good size uniformity after $\text{Zn}(\text{OH})_2$ coating onto Cu_2O (Fig. 1d–f). High-magnification SEM images in Fig. 1g–i display that $\text{Zn}(\text{OH})_2$ layers are tightly wrapped on the surfaces of Cu_2O with different morphologies to form about 1 μm -sized hydrangea. Fig. S1 shows the TEM images and

^{*} Corresponding author.

E-mail addresses: liuap@zstu.edu.cn, liuaiping1979@gmail.com (A. Liu).

EDS mapping of cubic $\text{Cu}_2\text{O}@Zn(\text{OH})_2$ composites. The Cu_2O appears the typical cubic shape (Fig. S1a). From the HRTEM image (Fig. S1b), the cubic Cu_2O surface is coated by a thin film perfectly, wherein the lattice sizes of 0.395, 0.354 and 0.418 nm are corresponding to the {100}, {102} and {111} facets of $\text{Zn}(\text{OH})_2$, respectively. The element distribution maps of the composites verify the existence of Cu, Zn and O elements (Fig. S1c–e), hinting the interior Cu_2O coated by $\text{Zn}(\text{OH})_2$ integrally.

Fig. 2 shows the XRD patterns of Cu_2O crystals and $\text{Cu}_2\text{O}@Zn(\text{OH})_2$ composites with three different morphologies. The curves of the three Cu_2O crystals are similar, but exhibit different {111} peak intensities, namely the peak intensity follows the order of octahedral Cu_2O > cuboctahedral Cu_2O > cubic Cu_2O . The $\text{Cu}_2\text{O}@Zn(\text{OH})_2$ composites also show similar intensity variation at {111} facet. In addition, the three composites display the characteristic peaks of $\text{Zn}(\text{OH})_2$ at 18.9° , 38.9° and 57.9° , corresponding to {001}, {002} and {110} facets of $\text{Zn}(\text{OH})_2$, respectively. As Cu_2O has good crystallinity, its diffraction peaks are stronger than those of $\text{Zn}(\text{OH})_2$. Combined with the crystal facet characterization (Fig. S1), it is confirmed that the $\text{Cu}_2\text{O}@Zn(\text{OH})_2$ composites are synthesized.

Fig. 3a shows the photocatalytic degradation percentage of MO by using Cu_2O and $\text{Cu}_2\text{O}@Zn(\text{OH})_2$ as catalyst materials. In the case of without light irradiation, the decrease in concentration of MO (the ratio of concentration at each irradiation time interval C and the one of the initial concentration C_0 at adsorption-desorption equilibrium) by using cuboctahedral $\text{Cu}_2\text{O}@Zn(\text{OH})_2$ can be attributed to the absorption of MO molecules on $\text{Zn}(\text{OH})_2$ nanosheets with unique structure due to no occurrence of photocatalytic degradation process. When the adsorption of MO reaches equilibrium, the concentration of MO does not change again. In addition, the photocatalytic degradation performances of three $\text{Cu}_2\text{O}@Zn(\text{OH})_2$ are compared, among which the cuboctahedral $\text{Cu}_2\text{O}@Zn(\text{OH})_2$ has the best photocatalytic degradation performance with the MO degradation rate as high as 96.6 % when compared to the cubic and octahedral $\text{Cu}_2\text{O}@Zn(\text{OH})_2$ as well as the single Cu_2O catalysts (Fig. 3a). This is mainly attributed to the following two points. Firstly, the efficient adsorption capacity of $\text{Zn}(\text{OH})_2$ can quickly adsorb the MO molecules and then supply them to Cu_2O surface for catalysis,

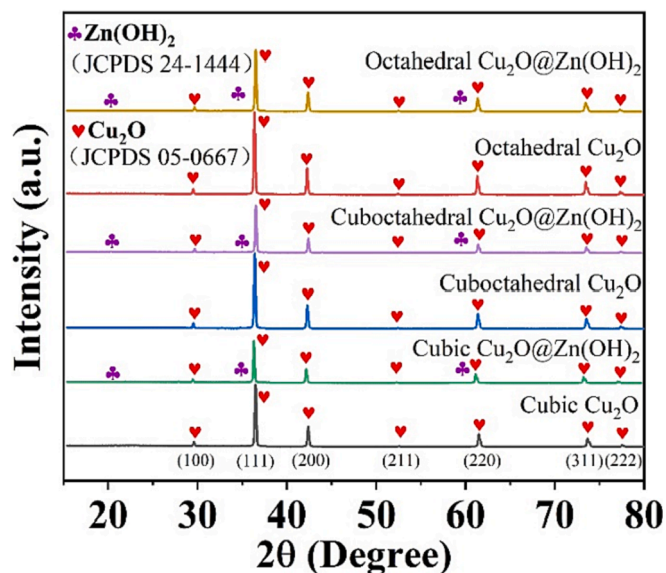


Fig. 2. XRD patterns of pure Cu_2O crystals with different morphologies and the corresponding $\text{Cu}_2\text{O}@Zn(\text{OH})_2$ composites.

which can make up the defect that the catalyst could not quickly contact with organic dye molecules, thus accelerating the catalytic reaction and improving the catalytic efficiency. Secondly, as the catalytic performance of low-index facet Cu_2O crystals follows the sequence of {110} > {111} > {100}, thus the octahedral Cu_2O with {111} facets exposed should possess a better catalytic activity than the cubic Cu_2O with {100} facets exposed [8,9]. The coexistence of {111} and {100} facets of cuboctahedral Cu_2O can induce better separation of charge carriers due to the slight difference in energy levels between the two planes, thus, the photo-generated electrons selectively aggregate on the {111} facets, and holes tend to shift to the {100} facets [10], resulting in the better catalytic activity than the octahedral Cu_2O with {111} facets.

The photoluminescence (PL) spectrum and transient photocurrent (I-

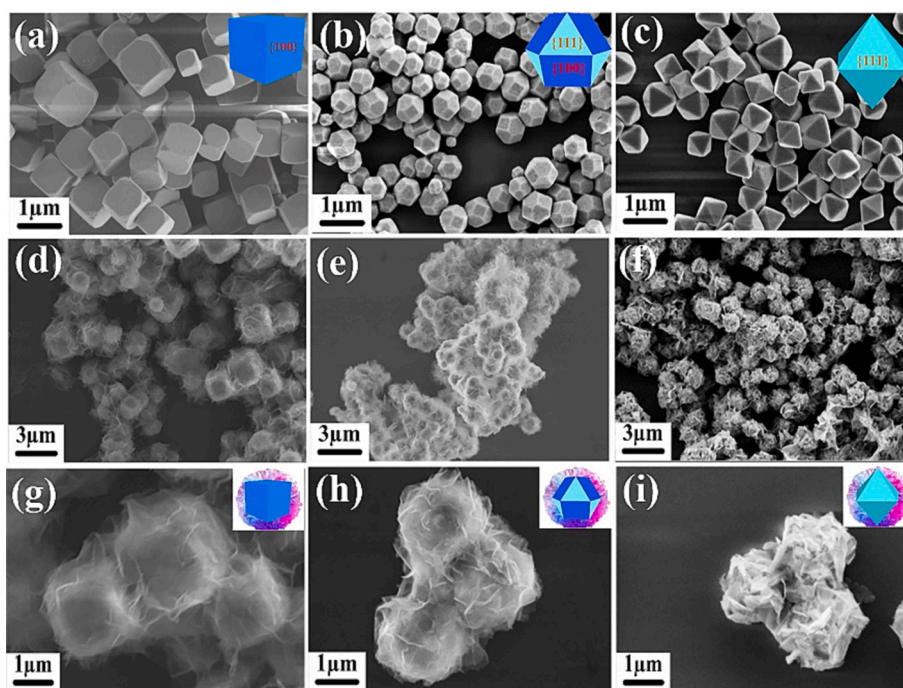


Fig. 1. SEM images of (a) cubic Cu_2O , (b) cuboctahedral Cu_2O , (c) octahedral Cu_2O , (d) cubic $\text{Cu}_2\text{O}@Zn(\text{OH})_2$, (e) cuboctahedral $\text{Cu}_2\text{O}@Zn(\text{OH})_2$, (f) octahedral $\text{Cu}_2\text{O}@Zn(\text{OH})_2$, high magnification SEM images of (g) cubic $\text{Cu}_2\text{O}@Zn(\text{OH})_2$, (h) cuboctahedral $\text{Cu}_2\text{O}@Zn(\text{OH})_2$, and (i) octahedral $\text{Cu}_2\text{O}@Zn(\text{OH})_2$.

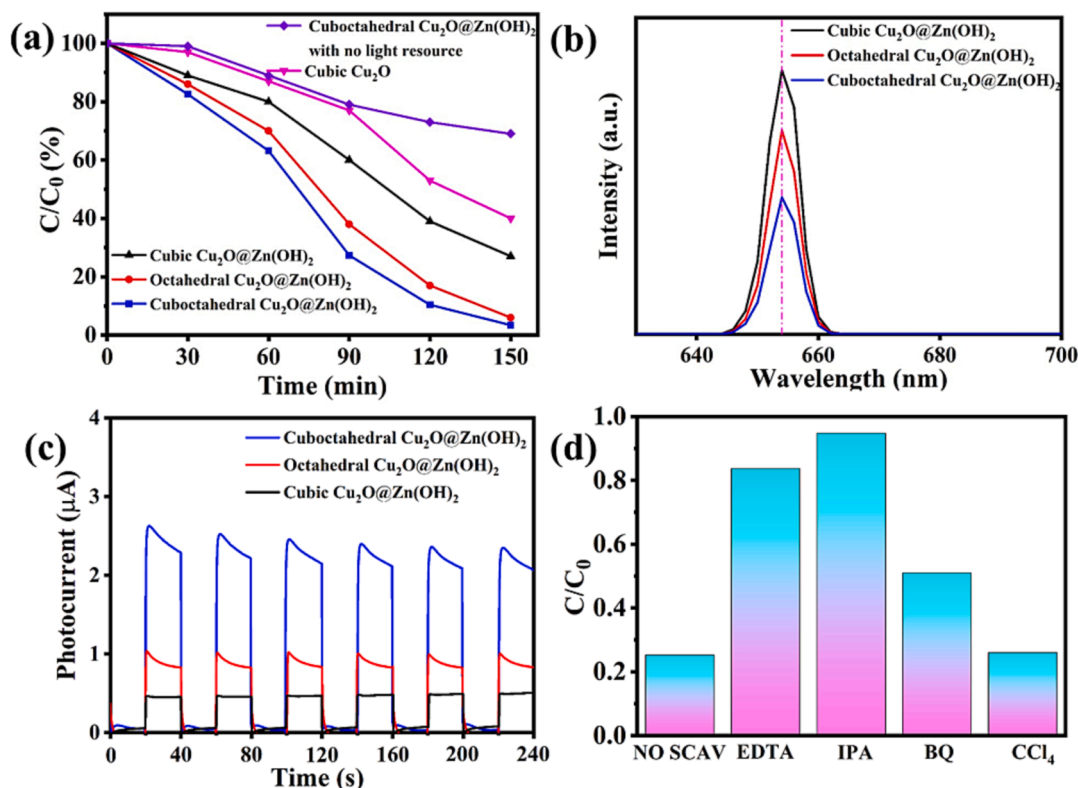


Fig. 3. Photocatalytic degradation of MO in the presence of various photocatalysts under visible-light irradiation: (a) photocatalytic degradation of MO as a function of irradiation time, (b) PL spectra, (c) I-T curves and (d) trapping experiment of active species during the photodegradation of MO in the presence of cuboctahedral $\text{Cu}_2\text{O}@Zn(\text{OH})_2$ photocatalyst and different scavengers.

T) curves also confirm that the cuboctahedral $\text{Cu}_2\text{O}@Zn(\text{OH})_2$ composite has the best electron-hole separation ability with the weakest PL peak intensity and biggest photo-generated current (Fig. 3b and c), indicating that the simultaneous existence of two facets provides a driving force for promoting electron-hole pair separation [11].

In order to better understand the catalytic degradation mechanism of $\text{Cu}_2\text{O}@Zn(\text{OH})_2$ to MO, reactive species scavenger method was carried out to confirm the main reactive species involved in the photocatalytic degradation process. The results indicate that $\cdot\text{OH}$ radicals and holes play the main roles in the photocatalytic degradation process, and some electrons would recombine with holes or react with molecular oxygen in the solution to generate a small quantity of $\cdot\text{O}_2^-$ (more details in Supporting information).

4. Conclusions

In summary, novel $\text{Cu}_2\text{O}@Zn(\text{OH})_2$ composites with different morphologies were prepared. The cuboctahedral $\text{Cu}_2\text{O}@Zn(\text{OH})_2$ composites with {100} and {111} facets of Cu_2O provided the driving force to promote the separation of electron-hole pairs, thus presented the best catalytic performance for the degradation of MO than the other two composites. In addition, the combination of $\text{Zn}(\text{OH})_2$ nanosheets with Cu_2O could further enhance the catalytic performance through the strong adsorption to MO. Thus, the synergy of $\text{Zn}(\text{OH})_2$ nanosheets with physical adsorption capacity and Cu_2O crystals with catalytic performance led to the enhanced photocatalytic performance of composite catalysts.

Declaration of Competing Interest

The authors declare that they have no known competing financial interests or personal relationships that could have appeared to influence the work reported in this paper.

Data availability

Data will be made available on request.

Acknowledgement

This work was supported by the National Natural Science Foundation of China (No. 12272351), the Youth Top-notch Talent Project of Zhejiang Ten Thousand Plan of China (No. ZJWR0308010), and the Zhejiang Provincial Natural Science Foundation of China (No. LR19E020004 and LQ20E010009).

Appendix A. Supplementary data

Supplementary data to this article can be found online at <https://doi.org/10.1016/j.matlet.2022.133334>.

References

- [1] Y.H. Zhang, M.M. Liu, J.L. Chen, S.M. Fang, P.P. Zhou, Dalton Trans. 50 (2021) 4091–4111.
- [2] S.D. Sun, X.J. Zhang, Q. Yang, S.H. Liang, X.Z. Zhang, Z.M. Yang, Prog. Mater. Sci. 96 (2018) 111–173.
- [3] Y.G. Gao, Q. Wu, X.Z. Liang, Z.Y. Wang, Z.K. Zheng, P. Wang, Y.Y. Liu, Y. Dai, M. H. Whangbo, B.B. Huang, Adv. Sci. 7 (2020) 1902820.
- [4] E.D. Kim, Y.S. Cho, Y.D. Huh, CrystEngComm 24 (2022) 3014–3019.
- [5] X. Chen, K. Cui, Z. Hai, W. Kuang, X. Tian, Mater. Lett. 297 (2021), 129921.
- [6] Y. Wu, S. Zeng, Y. Dong, Y. Fu, H. Sun, S. Yin, X. Guo, W. Qin, RSC Adv. 8 (2018) 11395–11402.
- [7] D.F. Zhang, Z. Hua, G. Lin, K. Zheng, Z. Zhang, J. Mater. Chem. 19 (2009) 5220–5225.
- [8] S.C. Wu, C.S. Tan, M.H. Huang, Adv. Funct. Mater. 27 (2017) 1604635.
- [9] W.C. Huang, L.M. Lyu, Y.C. Yang, M.H. Huang, J. Am. Chem. Soc. 134 (2012) 1261–1267.
- [10] L. Zhang, J. Shi, M. Liu, D. Jing, L. Guo, Chem. Comm. 50 (2014) 192–194.
- [11] Y. Shang, L. Guo, Adv. Sci. 2 (2015) 1500140.